Materials and Design 162 (2019) 229–234

Contents lists available at ScienceDirect

Materials and Design

journal homepage: www.elsevier.com/locate/matdes

Laser welding of precipitation strengthened Ni-rich NiTiHf high temperature shape memory alloys: Microstructure and mechanical properties

J.P. Oliveira [a,*], N. Schell [b], N. Zhou [c], L. Wood [d,1], O. Benafan [d]

[a] UNIDEMI, Departamento de Engenharia Mecânica e Industrial, Faculdade de Ciências e Tecnologia, Universidade Nova de Lisboa, Caparica, Portugal
[b] Institute of Materials Research, Helmholtz-Zentrum Geesthacht, Max-Planck-Str. 1, D-21502 Geesthacht, Germany
[c] Centre for Advanced Materials Joining, University of Waterloo, Canada
[d] NASA Glenn Research Center, Materials and Structures Division, Cleveland, OH 44135, USA

HIGHLIGHTS

- First report on welding of NiTiHf high temperature shape memory alloys
- Synchrotron X-ray diffraction was used for microstructural mapping.
- The welded joint exhibited shape memory effect and superelasticity comparable to the base material.

GRAPHICAL ABSTRACT

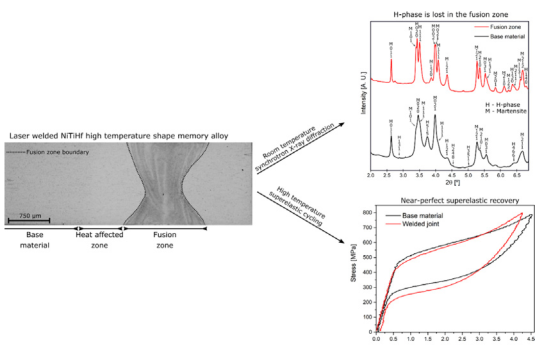

ARTICLE INFO

Article history:
Received 23 October 2018
Received in revised form 19 November 2018
Accepted 25 November 2018
Available online 27 November 2018

Keywords:
Laser welding
High temperature shape memory alloys
Martensitic phase transformation
Superelasticity
Synchrotron radiation
NiTiHf

ABSTRACT

High temperature shape memory alloys are currently attracting significant attention by the aerospace industry due to the potential use of shape memory and superelastic properties at temperatures above 100 °C. Virtually any advanced engineering material must, at some point, be joined either to itself, to create complex shaped structures, or to other materials to increase its potential applications. In this work, laser welding of a precipitation strengthened Ni-rich NiTiHf high temperature shape memory alloy is reported for the first time. Starting with a base material aged at 500 °C for 3 h and air cooled, defect-free joints with a conduction weld mode were obtained. Microstructural characterization, facilitated via microscopy and synchrotron X-ray diffraction, revealed that the fusion zone contained a single-phase martensitic structure at room temperature, compared to a mixture of martensite and H-phase precipitates in the base material. Isothermal loading in both the martensite (at 30 °C) and austenite (at 200 °C) phases revealed equivalent strength and near-perfect superelasticity in the welded and un-welded reference material.

1. Introduction

Shape memory alloys are a class of functional materials which exhibit a reversible martensitic phase transformation responsible for their shape memory and superelastic properties [1,2]. Among the

* Corresponding author.
E-mail address: jp.oliveira@fct.unl.pt (J.P. Oliveira).
[1] Student Intern: NASA Glenn Research Center, Materials and Structures Division, Cleveland, OH 44135, USA.

https://doi.org/10.1016/j.matdes.2018.11.053

several classes of shape memory alloys, NiTi is the most prevalent owing to its structural practicality and significant work output [3–5]. However, potential applications of this material are limited to a maximum operation temperature of 100 °C [6]. Significant research efforts have been made to address this limitation by developing high temperature shape memory alloys based on the Ni-Ti-X system [7–15]. Among the different alloys that have emerged, NiTiHf provides a low-cost alternative when compared to NiTiPd, NiTiAu or NiTiPt alloys [16,17]. Moreover, it was observed that Ni-rich NiTiHf shape memory alloys exhibit excellent mechanical properties and dimensional stability for precise compositional ranges and ageing conditions. It was shown that the solid-solution and precipitation strengthening via nanoscale H-phase precipitates [18–20] provide a high resistance to dislocation motion, while allowing an unobstructed path for the phase transformation to occur.

With the steady growth in the NiTiHf alloys research development in recent years, there is a need for complex geometries and shapes that cannot be obtained via conventional machining/processing. One way to expand this field and enable new applications is through the development of appropriate joining techniques for complex shapes or by additive manufacturing techniques [21–24]. While the latter have shown significant promise, the technology is still maturing at a slow pace given the multifaceted nature of these materials. On the other hand, several decades of research in welding technologies provide researchers an ideal tool for understanding the processing-microstructure-properties relationships arising from advanced manufacturing techniques in new materials. Welding of shape memory alloys have been reported for NiTi [23,25–28], Cu-based [29–31] and Fe-based [32,33] systems. Among the different joining techniques used, laser welding is currently the most used joining technique for shape memory alloys [34–39], owing to the precise control of the heat source and reduced extension of the thermally affected regions [29,40,41]. Critical to any joining technique applied to these materials is to preserve their functional properties, otherwise their intrinsic value may be lost.

To the best of the authors' knowledge there are currently no reported attempts in the literature on welding of high temperature shape memory alloys. In this work, laser welding of a precipitation strengthened NiTiHf shape memory alloy was performed. The microstructure of the welded joint was characterized by optical and electron microscopy methods and synchrotron X-ray diffraction. The mechanical response during tensile deformation at room and high temperature was also evaluated.

2. Experimental procedure

Ni-rich $Ni_{50.3}Ti_{29.7}Hf_{20}$ (at.%) was produced by vacuum induction skull melting (designated as FS#5). The ingots were vacuum homogenized at 1050 °C for 72 h followed by extrusion at 900 °C with an area reduction ratio of 7:1. Extruded rods were subjected to an ageing treatment of 3 h at 550 °C under argon, and then air-cooled, followed by final sample machining to a final rod diameter of 1.5 mm by 50.8 mm long.

Laser welding was performed using a Nd:YAG Miyachi Unitek LW50A system operating in pulsed wave mode with a top-hat profile. A 20 ms pulse with an energy of 39.9 J was used to obtain full penetration welds. The laser beam was focused on the surface of the NiTiHf base material with a diameter of 600 μm. Additional details of the laser welding setup can be found elsewhere [42]. To avoid oxidation, Ar was used as shielding gas at a flow rate of 0.57 m^3/h. Prior to welding, the base material was cleaned with acetone and alcohol to remove any impurities that could be detrimental to the welded joint.

After welding, the joints were polished for microstructural characterization by means of optical and scanning electron microscopy. Hardness measurements across the welded joints were performed using a load of 300 g and a hold time of 12 s. The space between consecutive indentations was 200 μm.

Structural characterization was performed using synchrotron X-ray diffraction at P07 beamline at DESY/PETRA III. The X-ray diffraction experiment was performed at room temperature working in transmission mode. A schematic representation of the experimental setup is depicted in Fig. 1.

A beam spot of 200 × 200 μm^2 was used to probe the joint from the base material to the heat affected zone and to the fusion zone, with a 200 μm step between each consecutive spot. The wavelength was 0.1423 Å (87 keV) and the sample-to-detector distance was set to 1527 mm. The 2D raw images were treated using Fit2D software as described in the literature [43,44].

Mechanical testing was performed on an MTS Insight load frame equipped with a MTS Advantage™ environmental chamber. The gauge length of the samples was 20 mm, which is approximately 10 times the length span of the fusion zone (refer to Fig. 2a). Temperature was measured using a digital Eurotherm controller and type-K thermocouples attached to the sample. Strain measurements were accomplished using a GOM ARAMIS digital image correlation (DIC) optical metrology system. A black and white speckle pattern was painted onto each specimen using high temperature paint. Data was processed using ARAMIS software and custom MATLAB® scripts. Tensile tests were performed in stress control at a rate of 40 MPa/min at room temperature and at 200 °C to probe the martensite and austenite phases, respectively. For reference, 200 °C was chosen based on austenite finish temperature plus 30 °C as determined by differential scanning calorimetry. The samples were loaded to 700 and 800 MPa (at room temperature and 200 °C, respectively) followed by unloading to a zero-stress condition. The base material was subjected to the same mechanical loading for comparison purposes.

3. Results and discussion

Cross-section view of the welded joint (Fig. 2a) reveals a fully penetrating joint with no welding defects, such as cracks or pores. As described elsewhere [45], during laser-based processing the control of the processing parameters is critical for the formation defects, or lack thereof. In laser welding, depending on the aspect ratio of the fusion zone, conduction or keyhole welding mode may occur. Based on the material thermophysical properties and laser characteristics different geometries in the fusion zone can be obtained [46]. Keyhole mode is identified when the aspect ratio of the fusion is ≫1. According to the obtained fusion zone geometry, an aspect ratio of ≈ 1 was obtained which is characteristic of a conduction mode welding. Moreover, keyhole mode welding, which is also identified by a deep and narrow fusion zone, is observed in laser welding [47] where temperatures are significantly higher than those observed in conduction mode welding. Since NiTi-based shape memory alloys are prone to elemental evaporation, which tends to drastically change their transformation characteristics

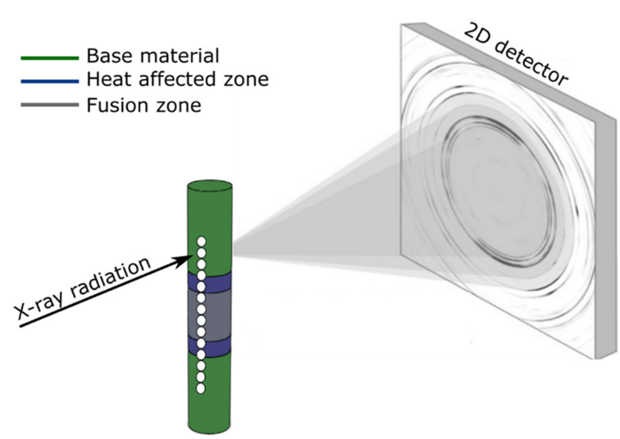

Fig. 1. Schematic representation of the synchrotron X-ray diffraction measurements across the welded specimen.

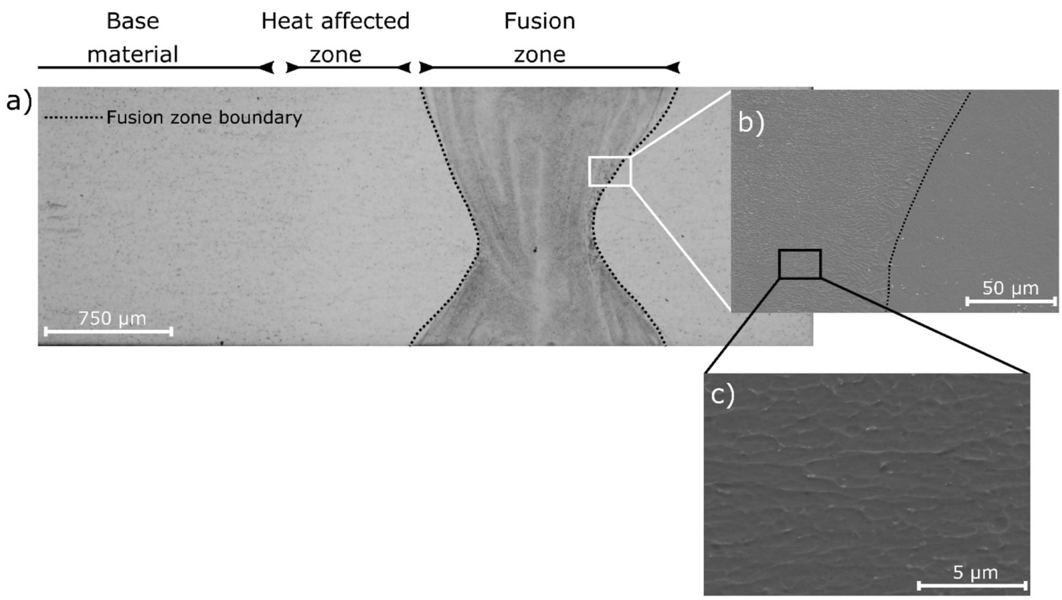

Fig. 2. a) Optical microscope image of the NiTiHf weld; b) Scanning electron microscope image of the fusion zone/heat affected zone boundary; c) high magnification image of the fusion zone.

[21,44], it is desirable that conduction weld is obtained, as seen in this work, to decrease the magnitude of such changes.

Fig. 2b depicts the fusion zone/heat affected zone interface, showing the presence of a dendritic network in the latter region, as evidenced by the high magnification scanning electron microscope image shown in Fig. 2c. Evidence of H-phase precipitates (identified by synchrotron X-ray diffraction as it will be presented later) are found in the heat affected zone, though these are not observed in the fusion zone of the welded joint.

Microhardness mapping across the joint was performed to evaluate the changes caused by the thermal cycle experienced by the material during welding. These results are depicted in Fig. 3. As it can be observed, the base material has the higher hardness, averaging roughly 490 HV, owing to the ageing heat treatment which promotes H-phase precipitation. However, the hardness values decrease in the heat affected zone to approximately 430 HV, and this decrease is even more drastic in the fusion zone decreasing to around 370 HV.

A superimposition of the X-ray diffraction patterns crossing all the regions of the welded joint (base material, heat affected zone and fusion zone) obtained using synchrotron radiation at room temperature is depicted in Fig. 4.

The diffraction patterns reveal a clear difference between the base material and the heat affected and fusion zones. To better elucidate on the microstructural-induced changes in the latter two regions, a representative pattern from each region of interest is depicted in Fig. 5.

As expected, at room temperature, the base material consisted of martensite and H-phase precipitates. For NiTiHf alloys it was found that ageing at 550 °C for 3 h gives rise to finely dispersed nanometer H-phase precipitation [48], which enhances the mechanical and functional properties of the material. This results in precipitation strengthening of the alloy, while limiting the accumulation of residual strain during thermo-mechanical loading. In the fusion zone, only martensite peaks are detected, but with a district texture (i.e., different peak intensities, and number of peaks). It is noted that during the thermomechanical processing of the base material, a well-defined texture is developed from the hot working and extrusion processes. However, re-melting and subsequent solidification in the fusion zone removes the effect of previous thermomechanical processing. Therefore, the existence of new diffraction peaks of martensite in the fusion zone suggests that the texture of the extruded base material was lost or reduced. This can be related to the solidification conditions observed in fusion welding, which can promote preferential orientation of the grain structure [49,50].

The presence of a fully martensitic structure in the fusion zone, in contrast to the dual martensite/H-phase structure of the base material, further validates the decrease in hardness in the former region. In fact, for a fully homogenized NiTiHf alloy, (i.e., no H-phase precipitates), the hardness was measured to be 350 HV, approaching the 370 HV value measured here. In the fusion zone, the melting and subsequent fast cooling of the material resulted in a precipitate-free region, similar to the homogenized base material.

In the heat affected zone, the weld thermal cycle promotes grain growth and partial dissolution of the H-phase precipitates [51] close to the fusion boundary, hence resulting in lower hardness compared to the non-affected base material. This softening effect in the heat affected zone was also observed in laser welded joints of the NiTi system [52,53]. However, it must be noticed that in the heat affected zone closer to the base material, the weld thermal cycle is not enough to promote

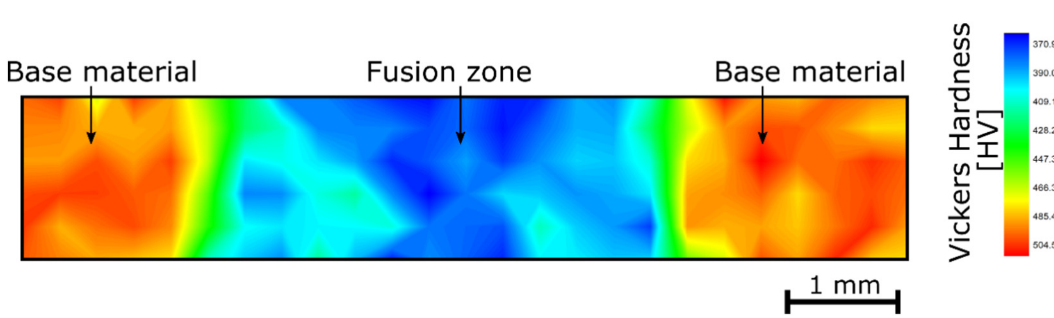

Fig. 3. Microhardness mapping of the NiTiHf laser welded joint.

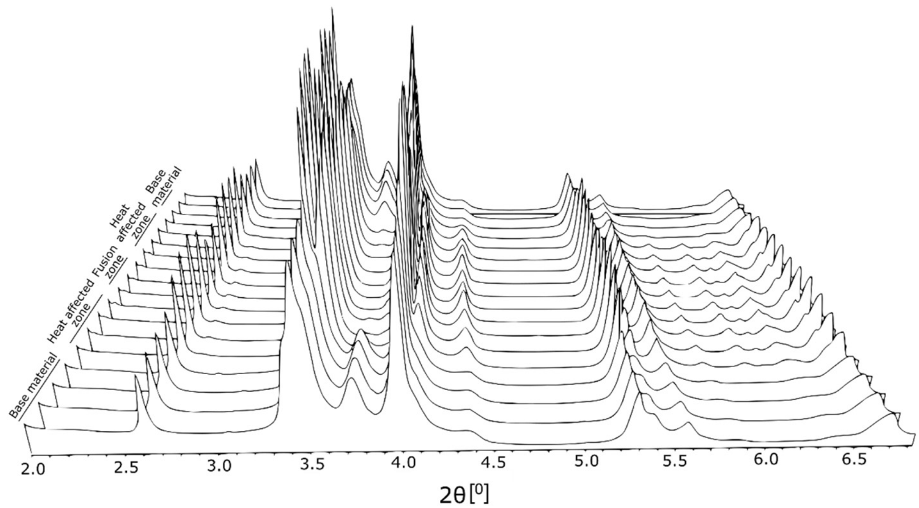

Fig. 4. Superimposition of X-ray diffraction patterns of the welded joint.

the complete dissolution of H-phase, as evidenced in the diffraction pattern corresponding to this region presented in Fig. 5. This results in higher hardness values compared to the precipitate-free regions. Closer to the fusion zone, where the peak temperatures increase, H-phase dissolution is more effective resulting in a precipitate-free region.

To evaluate the influence of laser welding on the mechanical properties of the joint, a load/unload cycle at both room temperature and 200 °C was performed and compared to the base material. These results are depicted in Fig. 6a and b, respectively. Remarkably, despite the microstructural modifications, which occurred in the fusion zone, there are no significant changes in the mechanical behavior of the welded joints up to the tested loads. At room temperature, the material exhibited the classical stress-strain curve for these alloys [54] where the base material deformed slightly more (1.74% compared to 1.62%) up to the maximum tensile stress of 700 MPa. The elastic moduli were calculated to be 58 and 56 GPa, for the base and welded samples, respectively. Loading

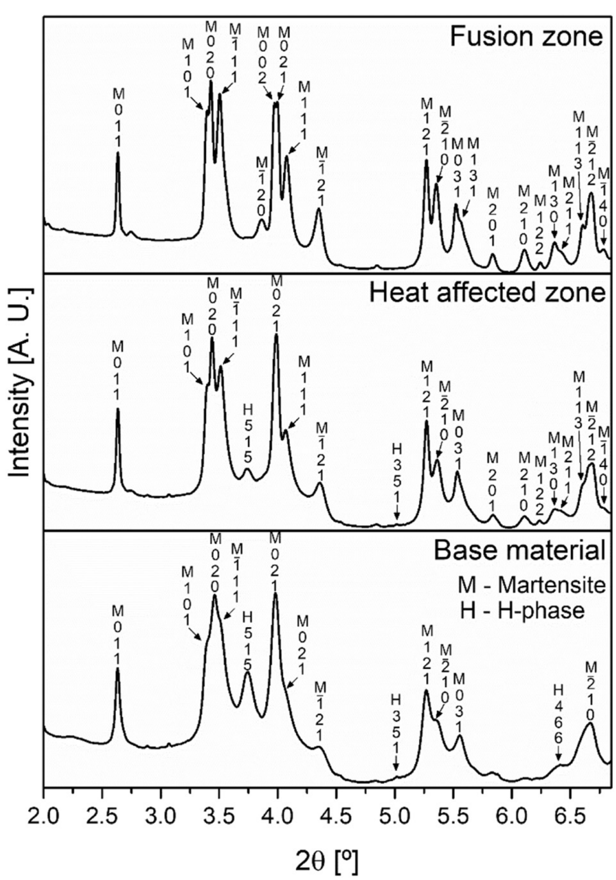

Fig. 5. Representative X-ray diffraction patterns from the base material, heat affected zone and fusion zone.

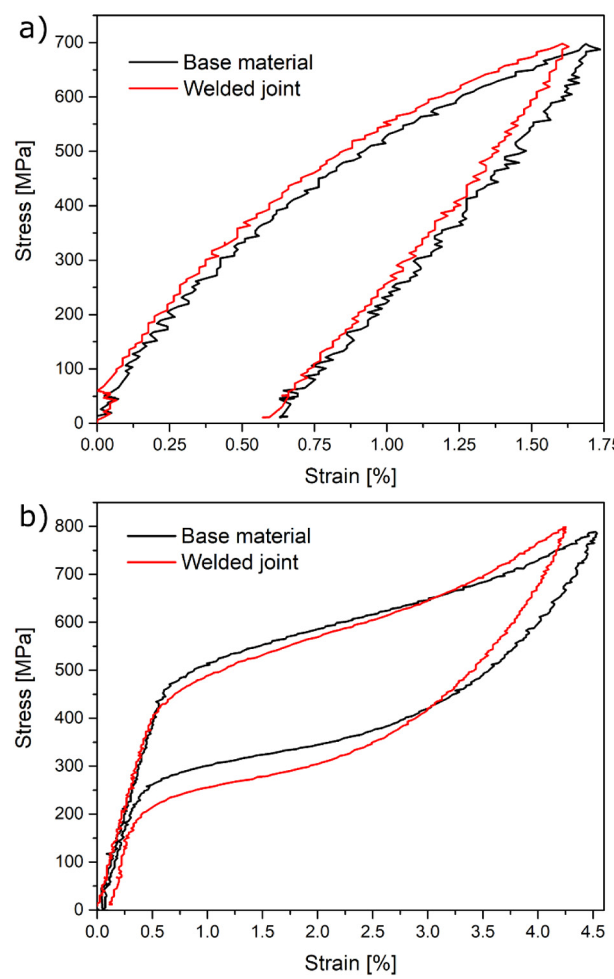

Fig. 6. Load/unload of the welded joint and base material at: a) room temperature; b) 200 °C.

beyond the elastic region into the reorientation and detwinning segment, including the unloading curves, showed near identical behavior. At high temperature, a classical superelastic curve was obtained with similar observations between the base and welded material (4.54% compared to 4.23% at max stress). The austenite elastic moduli were found to be 81 and 78 GPa, for the base and welded samples, respectively. It is noted that these small variations in strain may be due to nature of testing and not necessarily due to the integrity of the weld. In both cases (low and high temperature), all the strains were fully recovered upon heating for the case of room temperature test, triggering the shape memory effect, and upon unloading for the superelastic test. The nearly negligible change in the mechanical properties of the welded joint when compared to the base material can be justified by the unique characteristics of laser welding, where it is possible to concentrate the heat to promote joining in a very restrict region of the material, thus minimizing the potentially detrimental effects of the thermal cycle on the microstructural and mechanical characteristics of the joint.

Of special interest in these joints is the fact that the high temperature superelastic behavior after welding was not affected, with a typical superelastic curve for these alloys being observed. The absorbed energy during superelastic cycling was higher for the welded joint (8.45 MJ/m^3 vs 8.16 MJ/m^3). The onset for the forward transformation, occurred at 480 MPa for the base material and at 450 MPa for the joint, while the reverse transformation was observed at 450 and 380 MPa, respectively. This slight change, which can be attributed to the softening effect of the heat affected and fusion zones [52], increasing the hysteretic loop area, hence contributing to a higher amount of energy absorbed by the welded joint. It is also noted that the welded sample exhibited a small (0.12%) but higher residual strains upon unloading, commensurate with the effectively un-aged fusion zone that contribute to this effect. The high slope during the stress induced transformation observed in both specimens is typical of NiTiHf alloys [48]. It is noted that tests were limited to a single cycle at 700 and 800 MPa in this study, it is possible that higher stresses may have different outcomes. However, it is expected that most applications will be at or below this already high stresses for the most part. Additional tests regarding thermal cycling of the welded material under load are underway.

4. Conclusions

Welding of a Ni-rich $Ni_{50.3}Ti_{29.7}Hf_{20}$ (at.%) shape memory alloy is reported for the first time. Defect-free laser welded joints were obtained while achieving a conduction mode welding. In the fusion zone, a single-phase martensitic structure was observed at room temperature, which contrasts with the heat-treated base material, which was composed of a mixture of martensite and H-phase precipitates. In the heat affected zone partial dissolution of H-phase occurred leading to material softening and a hardness decrease. Despite the microstructural changes, the welded joint exhibited similar mechanical properties to those of the base material. In fact, load/unload testing at room and high temperature revealed a stress-strain response with near zero residual strains. Near perfect superelasticity was observed in the high temperature cycling for the welded joint, opening new potential applications for these materials in aerospace applications. In summary, the ability of laser welding to confine the heat in a small region of the material, while promote joining, can preserve the functional properties of the alloy, despite the microstructural changes in the fusion zone.

CRediT authorship contribution statement

J.P. Oliveira: Conceptualization, Formal analysis, Investigation, Data curation, Writing - original draft, Writing - review & editing. **N. Schell:** Investigation, Data curation, Writing - review & editing. **N. Zhou:** Resources, Investigation, Writing - review & editing. **L. Wood:** Investigation, Data curation. **O. Benafan:** Investigation, Data curation, Writing - original draft, Writing - review & editing.

Acknowledgments

JPO acknowledges Fundação para a Ciência e a Tecnologia (FCT - MCTES) for its financial support via the project PEst-OE/EME/UI0667/2014 and DESY via beamtime proposal I-20160912. Funding from the NASA Aeronautics Research Mission Directorate (ARMD) Transformational Tools & Technologies (TTT) project is gratefully acknowledged.

The raw/processed data required to reproduce these findings cannot be shared at this time as the data also forms part of an ongoing study.

References

[1] K. Otsuka, X. Ren, Physical metallurgy of Ti-Ni-based shape memory alloys, Prog. Mater. Sci. 50 (2005) 511–678, https://doi.org/10.1016/j.pmatsci.2004.10.001.
[2] J.M. Jani, M. Leary, A. Subic, M.A. Gibson, J. Mohd Jani, M. Leary, A. Subic, M.A. Gibson, A review of shape memory alloy research, applications and opportunities, Mater. Des. 56 (2014) 1078–1113, https://doi.org/10.1016/j.matdes.2013.11.084.
[3] M. Elahinia, N. Shayesteh Moghaddam, M. Taheri Andani, A. Amerinatanzi, B.A. Bimber, R.F. Hamilton, Fabrication of NiTi through additive manufacturing: a review, Prog. Mater. Sci. 83 (2016) 630–663, https://doi.org/10.1016/j.pmatsci.2016.08.001.
[4] L. Petrini, F. Migliavacca, Biomedical applications of shape memory alloys, J. Metall. 2011 (2011) 1–15, https://doi.org/10.1155/2011/501483.
[5] J. Van Humbeeck, Damping capacity of thermoelastic martensite in shape memory alloys, J. Alloys Compd. 355 (2003) 58–64, https://doi.org/10.1016/S0925-8388(03)00268-8.
[6] J. Van Humbeeck, Non-medical applications of shape memory alloys, Mater. Sci. Eng. A 273–275 (1999) 134–148, https://doi.org/10.1016/S0921-5093(99)00293-2.
[7] L. Casalena, J.M. Sosa, D.R. Coughlin, F. Yang, X. Chen, H. Paranjape, Y. Gao, R.D. Noebe, G.S. Bigelow, D.J. Gaydosh, S.A. Padula, Y. Wang, P.M. Anderson, M.J. Mills, Revealing transformation and deformation mechanisms in NiTiHf and NiTiAu high temperature shape memory alloys through microstructural investigations, Microsc. Microanal. 22 (2016) 1954–1955, https://doi.org/10.1017/S1431927616010618.
[8] L. Patriarca, H. Sehitoglu, E.Y. Panchenko, Y.I. Chumlyakov, High-temperature functional behavior of single crystal Ni51.2Ti23.4Hf25.4 shape memory alloy, Acta Mater. 106 (2016) 333–343, https://doi.org/10.1016/j.actamat.2016.01.015.
[9] Y. Wu, L. Patriarca, H. Sehitoglu, Y. Chumlyakov, Ultrahigh tensile transformation strains in new Ni 50.5 Ti 36.2 Hf 13.3 shape memory alloy, Scr. Mater. 118 (2016) 51–54, https://doi.org/10.1016/j.scriptamat.2016.03.009.
[10] H. Sehitoglu, Y. Wu, L. Patriarca, Shape memory functionality under multi-cycles in NiTiHf, Scr. Mater. 129 (2017) 11–15, https://doi.org/10.1016/j.scriptamat.2016.10.009.
[11] L. Casalena, G.S. Bigelow, Y. Gao, O. Benafan, R.D. Noebe, Y. Wang, M.J. Mills, Mechanical behavior and microstructural analysis of NiTi-40Au shape memory alloys exhibiting work output above 400 °C, Intermetallics 86 (2017) 33–44, https://doi.org/10.1016/j.intermet.2017.03.005.
[12] M. Carl, B. Van Doren, M.L. Young, In situ synchrotron radiation X-ray diffraction study on phase and oxide growth during a high temperature cycle of a NiTi-20 at.% Zr high temperature shape memory alloy, Shape Mem. Superelasticity 4 (2018) 174–185, https://doi.org/10.1007/s40830-018-0149-0.
[13] C.M. Denowh, D.A. Miller, Thermomechanical training and characterization of NiTiHf and NiTiHfCu high temperature shape memory alloys, Smart Mater. Struct. 21 (2012)https://doi.org/10.1088/0964-1726/21/6/065020.
[14] W. Cai, X.L. Meng, L.C. Zhao, Recent development of TiNi-based shape memory alloys, Curr. Opin. Solid State Mater. Sci. 9 (2005) 296–302, https://doi.org/10.1016/j.cossms.2006.07.002.
[15] R. Santamarta, R. Arróyave, J. Pons, A. Evirgen, I. Karaman, H.E. Karaca, R.D. Noebe, TEM study of structural and microstructural characteristics of a precipitate phase in Ni-rich Ni-Ti-Hf and Ni-Ti-Zr shape memory alloys, Acta Mater. 61 (2013) 6191–6206, https://doi.org/10.1016/j.actamat.2013.06.057.
[16] J. Ma, I. Karaman, R.D. Noebe, High temperature shape memory alloys, Int. Mater. Rev. 55 (2010) 257–315, https://doi.org/10.1179/095066010X12646898728363.
[17] D. Canadinc, W. Trehern, H. Ozcan, C. Hayrettin, O. Karakoc, I. Karaman, F. Sun, Z. Chaudhry, On the deformation response and cyclic stability of Ni 50 Ti 35 Hf 15 high temperature shape memory alloy wires, Scr. Mater. 135 (2017) 92–96, https://doi.org/10.1016/j.scriptamat.2017.03.025.
[18] F. Yang, D.R. Coughlin, P.J. Phillips, L. Yang, A. Devaraj, L. Kovarik, R.D. Noebe, M.J. Mills, Structure analysis of a precipitate phase in an Ni-rich high-temperature NiTiHf shape memory alloy, Acta Mater. 61 (2013) 3335–3346, https://doi.org/10.1016/j.actamat.2013.02.023.
[19] S.M. Saghaian, H.E. Karaca, H. Tobe, A.S. Turabi, S. Saedi, S.E. Saghaian, Y.I. Chumlyakov, R.D. Noebe, High strength NiTiHf shape memory alloys with tailorable properties, Acta Mater. 134 (2017) 211–220, https://doi.org/10.1016/j.actamat.2017.05.065.
[20] H.E. Karaca, S.M. Saghaian, G. Ded, H. Tobe, B. Basaran, H.J. Maier, R.D. Noebe, Y.I. Chumlyakov, Effects of nanoprecipitation on the shape memory and material properties of an Ni-rich NiTiHf high temperature shape memory alloy, Acta Mater. 61 (2013) 7422–7431, https://doi.org/10.1016/j.actamat.2013.08.048.
[21] J.P. Oliveira, A.J. Cavaleiro, N. Schell, A. Stark, R.M. Miranda, J.L. Ocana, F.M. Braz Fernandes, Effects of laser processing on the transformation characteristics of NiTi: a contribute to additive manufacturing, Scr. Mater. 152 (2018) 122–126, https://doi.org/10.1016/j.scriptamat.2018.04.024.
[22] M. Elahinia, N. Shayesteh Moghaddam, A. Amerinatanzi, S. Saedi, G.P. Toker, H. Karaca, G.S. Bigelow, O. Benafan, Additive manufacturing of NiTiHf high

temperature shape memory alloy, Scr. Mater. 145 (2018) 90–94, https://doi.org/10.1016/j.scriptamat.2017.10.016.
[23] D. Yang, H.C. Jiang, M.J. Zhao, L.J. Rong, Microstructure and mechanical behaviors of electron beam welded NiTi shape memory alloys, Mater. Des. 57 (2014) 21–25, https://doi.org/10.1016/j.matdes.2013.12.039.
[24] H.M. Li, D.Q. Sun, X.L. Cai, P. Dong, W.Q. Wang, Laser welding of TiNi shape memory alloy and stainless steel using Ni interlayer, Mater. Des. 39 (2012) 285–293, https://doi.org/10.1016/j.matdes.2012.02.031.
[25] V. Delobelle, P. Delobelle, Y. Liu, D. Favier, H. Louche, Resistance welding of NiTi shape memory alloy tubes, J. Mater. Process. Technol. 213 (2013) 1139–1145, https://doi.org/10.1016/j.jmatprotec.2013.01.013.
[26] C.W. Chan, H.C. Man, Laser welding of thin foil nickel–titanium shape memory alloy, Opt. Lasers Eng. 49 (2011) 121–126, https://doi.org/10.1016/j.optlaseng.2010.08.007.
[27] P. Burdet, J. Vannod, A. Hessler-Wyser, M. Rappaz, M. Cantoni, Three-dimensional chemical analysis of laser-welded NiTi–stainless steel wires using a dual-beam FIB, Acta Mater. 61 (2013) 3090–3098, https://doi.org/10.1016/j.actamat.2013.01.069.
[28] G. Fox, R. Hahnlen, M.J. Dapino, Fusion welding of nickel-titanium and 304 stainless steel tubes: part II: tungsten inert gas welding, J. Intell. Mater. Syst. Struct. 24 (2013) 962–972, https://doi.org/10.1177/1045389X12461076.
[29] J.P. Oliveira, Z. Zeng, S. Berveiller, D. Bouscaud, F.M. Braz Fernandes, R.M. Miranda, N. Zhou, Laser welding of Cu-Al-Be shape memory alloys: microstructure and mechanical properties, Mater. Des. 148 (2018) 145–152, https://doi.org/10.1016/j.matdes.2018.03.066.
[30] C.A. Biffi, B. Previtali, A. Tuissi, Microstructure and calorimetric behavior of laser welded open cell foams in CuZnAl shape memory alloy, Funct. Mater. Lett. 9 (2016), 1642007. https://doi.org/10.1142/S1793604716420078.
[31] C.A. Biffi, R. Casati, B. Previtali, A. Tuissi, Microstructure and mechanical properties of laser welded beads realized for joining CuZn open cellular foams, Mater. Lett. 181 (2016) 132–135, https://doi.org/10.1016/j.matlet.2016.05.161.
[32] P. Krooß, J. Günther, L. Halbauer, M. Vollmer, A. Buchwalder, R. Zenker, H. Biermann, T. Niendorf, Electron beam welding of Fe–Mn–Al–Ni shape memory alloy: microstructure evolution and shape memory response, Funct. Mater. Lett. 10 (2017), 1750043. https://doi.org/10.1142/S1793604717500436.
[33] H.C. Lin, K.M. Lin, Y.C. Chuang, T.S. Chou, The welding characteristics of Fe–30Mn–6Si and Fe–30Mn–6Si–5Cr shape memory alloys, J. Alloys Compd. 306 (2000) 186–192, https://doi.org/10.1016/S0925-8388(00)00762-3.
[34] J.P. Oliveira, R.M. Miranda, F.M. Braz Fernandes, Welding and joining of NiTi shape memory alloys: a review, Prog. Mater. Sci. 88 (2017) 412–466, https://doi.org/10.1016/j.pmatsci.2017.04.008.
[35] C.W. Chan, H.C. Man, Reduction of environmentally induced cracking of laser-welded shape memory NiTi wires via post-weld heat-treatment, Mater. Sci. Eng. A 588 (2013) 388–394, https://doi.org/10.1016/j.msea.2013.09.051.
[36] J. Vannod, M. Bornert, J.-E. Bidaux, L. Bataillard, A. Karimi, J.-M. Drezet, M. Rappaz, A. Hessler-Wyser, Mechanical and microstructural integrity of nickel–titanium and stainless steel laser joined wires, Acta Mater. 59 (2011) 6538–6546, https://doi.org/10.1016/j.actamat.2011.06.031.
[37] C.H. Ng, E.S.H. Mok, H.C. Man, Effect of Ta interlayer on laser welding of NiTi to AISI 316L stainless steel, J. Mater. Process. Technol. 226 (2015) 69–77, https://doi.org/10.1016/j.jmatprotec.2015.06.039.
[38] A. Shojaei Zoeram, S.A.A. Akbari Mousavi, Effect of interlayer thickness on microstructure and mechanical properties of as welded Ti6Al4V/Cu/NiTi joints, Mater. Lett. 133 (2014) 5–8, https://doi.org/10.1016/j.matlet.2014.06.141.
[39] H. Gugel, A. Schuermann, W. Theisen, Laser welding of NiTi wires, Mater. Sci. Eng. A 481–482 (2008) 668–671, https://doi.org/10.1016/j.msea.2006.11.179.
[40] W.M. Steen, J. Mazumder, Laser Material Processing, Springer London, London, 2010https://doi.org/10.1007/978-1-84996-062-5.
[41] S.V. Kuryntsev, A.E. Morushkin, A.K. Gilmutdinov, Fiber laser welding of austenitic steel and commercially pure copper butt joint, Opt. Lasers Eng. 90 (2017) 101–109, https://doi.org/10.1016/j.optlaseng.2016.10.008.
[42] J.P. Oliveira, B. Panton, Z. Zeng, T. Omori, Y. Zhou, R.M. Miranda, F.M. Braz Fernandes, Laser welded superelastic Cu–Al–Mn shape memory alloy wires, Mater. Des. 90 (2016) 122–128, https://doi.org/10.1016/j.matdes.2015.10.125.
[43] A.P. Hammersley, S.O. Svensson, M. Hanfland, A.N. Fitch, D. Hausermann, Two-dimensional detector software: from real detector to idealised image or two-theta scan, High Pressure Res. 14 (1996) 235–248, https://doi.org/10.1080/08957959608201408.
[44] J.P. Oliveira, F.M. Braz Fernandes, R.M. Miranda, N. Schell, J.L. Ocaña, Effect of laser welding parameters on the austenite and martensite phase fractions of NiTi, Mater. Charact. 119 (2016) 148–151, https://doi.org/10.1016/j.matchar.2016.08.001.
[45] H. Wu, J. Ren, Q. Huang, X. Zai, L. Liu, C. Chen, S. Liu, X. Yang, R. Li, Effect of laser parameters on microstructure, metallurgical defects and property of AlSi10Mg printed by selective laser melting, J. Micromechanics Mol. Phys. 02 (2017), 1750017. https://doi.org/10.1142/S2424913017500175.
[46] J. Liu, E. Stevens, Q. Yang, M. Chmielus, A.C. To, An analytical model of the melt pool and single track in coaxial laser direct metal deposition (LDMD) additive manufacturing, J. Micromechanics Mol. Phys. 02 (2017), 1750013. https://doi.org/10.1142/S2424913017500138.
[47] H.L. Wei, J.W. Elmer, T. Debroy, Crystal growth during keyhole mode laser welding, Acta Mater. 133 (2017) 10–20, https://doi.org/10.1016/j.actamat.2017.04.074.
[48] H.E. Karaca, E. Acar, H. Tobe, S.M. Saghaian, NiTiHf-based shape memory alloys, Mater. Sci. Technol. 30 (2014) 1530–1544, https://doi.org/10.1179/1743284714Y.0000000598.
[49] J.W. Park, S.S. Babu, J.M. Vitek, E.A. Kenik, S.A. David, Stray grain formation in single crystal Ni-base superalloy welds, J. Appl. Phys. 94 (2003) 4203–4209, https://doi.org/10.1063/1.1602950.
[50] S.A. David, J.M. Vitek, Correlation between solidification parameters and weld microstructures, Int. Mater. Rev. 34 (1989) 213–245, https://doi.org/10.1179/imr.1989.34.1.213.
[51] E. Panchenko, N. Surikov, Y. Chumlyakov, A. Eftifeeva, A. Neiman, H. Sehitoglu, Stress-ageing effects on the functional properties of high-strength [001]-oriented Ni51·0Ti37·3Hf12.5 single crystals, Mater. Today Proc. 4 (2017) 4778–4783. doi: https://doi.org/10.1016/j.matpr.2017.04.070.
[52] A. Tuissi, S. Besseghini, T. Ranucci, F. Squatrito, M. Pozzi, Effect of Nd-YAG laser welding on the functional properties of the Ni–49.6 at.%Ti, Mater. Sci. Eng. A 273–275 (1999) 813–817, https://doi.org/10.1016/S0921-5093(99)00422-0.
[53] A. Falvo, F.M.M. Furgiuele, C. Maletta, Laser welding of a NiTi alloy: mechanical and shape memory behaviour, Mater. Sci. Eng. A 412 (2005) 235–240, https://doi.org/10.1016/j.msea.2005.08.209.
[54] O. Benafan, A. Garg, R.D. Noebe, G.S. Bigelow, S.A. Padula, D.J. Gaydosh, N. Schell, J.H. Mabe, R. Vaidyanathan, Mechanical and functional behavior of a Ni-rich Ni50·3Ti29·7Hf20 high temperature shape memory alloy, Intermetallics 50 (2014) 94–107, https://doi.org/10.1016/j.intermet.2014.02.006.